

## **LETTER**

## MOCVD grown $\beta\text{-}\mathrm{Ga_2O_3}$ metal-oxide-semiconductor field effect transistors on sapphire

To cite this article: Ji-Hyeon Park et al 2019 Appl. Phys. Express 12 095503

View the <u>article online</u> for updates and enhancements.

## LETTER

## MOCVD grown $\beta$ -Ga<sub>2</sub>O<sub>3</sub> metal-oxide-semiconductor field effect transistors on sapphire



Ji-Hyeon Park 🗓, Ryan McClintock, Alexandre Jaud, Arash Dehzangi 🗓, and Manijeh Razeghi 🗓

Center for Quantum Devices, Department of Electrical and Computer Engineering, Northwestern University, Evanston, Illinois 60208, United States of America

\*E-mail: razeghi@eecs.northwestern.edu

Received July 18, 2019; revised August 9, 2019; accepted August 13, 2019; published online August 27, 2019

We fabricated β-Ga<sub>2</sub>O<sub>3</sub>:Si metal-oxide field-effect transistors (MOSFETs) on c-plane sapphire substrates which typically showed maximum drain current of 100 mA mm<sup>-1</sup>.  $\beta$ -Ga<sub>2</sub>O<sub>3</sub>:Si thin films were realized on c-plane sapphire substrates through a combination of metalorganic chemical vapor deposition and post-annealing. The MOSFET device presented excellent on/off drain current ratio of ~1011 with very low gate leakage current, sharp pinch off behavior, and a breakdown voltage of 400 V at  $V_G = -40$  V. The growth and fabrication of  $\beta$ -Ga<sub>2</sub>O<sub>3</sub>:Si MOSFETs on c-plane sapphire is valuable to its demonstration of the great potential for future high-power electronic devices.

© 2019 The Japan Society of Applied Physics

-Ga<sub>2</sub>O<sub>3</sub> has various applications like solar blind photodetectors; however, where it holds the most potential is the area of high power electronic devices. 1-7) The global need for stable and clean energy supplies in the near future motivates the fast development of high-power electronics with efficient energy conversion and utilization. Wide-bandgap semiconductors such as SiC and GaN are currently the best candidates to realize those high-power devices. They have high breakdown voltage and lower losses than existing silicon-based devices. However, those materials are expensive, requiring high-quality substrates, hence unideal for mass production. With an ultra-wide bandgap of ~4.9 eV and very large electrical breakdown field strength of ~8 MV cm<sup>-1</sup>, outperforming SiC and GaN,  $\beta$ -gallium oxide ( $\beta$ -Ga<sub>2</sub>O<sub>3</sub>) is considered a promising next generation semiconductor materials for power electronics. Its Baliga's power device figure of merit is estimated to be 3444, several times larger than those of 4H-SiC (340) and GaN (870), projecting higher breakdown voltages and efficiencies for  $\beta$ -Ga<sub>2</sub>O<sub>3</sub> power devices.<sup>8)</sup> Another important property of β-Ga<sub>2</sub>O<sub>3</sub> is that native substrates can be processed from bulk single crystals fabricated by the same melt-growth mechanisms employed for the production of sapphire substrates.

Nowadays, large and high-quality sapphire substrates are manufactured for low prices and in numbers comparable to those for silicon. As a result, one can expect that melt grown β-Ga<sub>2</sub>O<sub>3</sub> substrates will reap the same benefits. Recently, high quality  $\beta$ -Ga<sub>2</sub>O<sub>3</sub> have become achievable by homoepitaxy, which has opened the way of  $\beta$ -Ga<sub>2</sub>O<sub>3</sub> materials for real-world applications.<sup>9,10)</sup> However, at this stage, the technology is still limited by the lack of supply of low-cost homo substrates, which hinders the development of growth and fabrication based on  $\beta$ -Ga<sub>2</sub>O<sub>3</sub>. In order to solve this problem, it is useful to develop the growth of high quality β-Ga<sub>2</sub>O<sub>3</sub> on low-cost foreign substrates such as sapphire or silicon. 11,12)

Ga<sub>2</sub>O<sub>3</sub>-based high power transistors that have been actively reported in the literature are thin ( $\sim$ 200–300 nm) and lowdoped channels fabricated using silicon-ion implantation and doping by epitaxial growth techniques like molecular beam epitaxy (MBE) or metalorganic chemical vapor deposition (MOCVD). 13-17) Mechanical exfoliation has also been used to realize metal oxide semiconductor field effect transistors (MOSFETs) based on  $\beta$ -Ga<sub>2</sub>O<sub>3</sub> nanostructures. <sup>18–20)</sup>

However, as far as we know, there are no reports of β-Ga<sub>2</sub>O<sub>3</sub> based MOSFETs on sapphire substrates as a potential high-power device. In this letter, we report the demonstration and characterization of *n*-type  $\beta$ -Ga<sub>2</sub>O<sub>3</sub>:Si thin film MOSFETs on c-plane sapphire substrates in order to present a possibility for its potential application in highpower devices. To realize the  $\beta$ -Ga<sub>2</sub>O<sub>3</sub> thin film, a metastable κ-Ga<sub>2</sub>O<sub>3</sub>:Si thin films grown by MOCVD on c-plane sapphire substrates were phase-transformed to β-Ga<sub>2</sub>O<sub>3</sub>:Si through high-temperature rapid thermal annealing (RTA).

commercial horizontal-flow **MOCVD** (AIXTRON 200/4 RF) was used to grow Ga<sub>2</sub>O<sub>3</sub>:Si thin films on c-plane sapphire substrates at growth temperatures of 670 °C using trimethylgallium (TMGa) and high purity deionized water as the gallium and oxygen precursors, respectively. H<sub>2</sub> was used as the carrier gas. TMGa and water were injected into the reactor via separate manifolds and isolated within the chamber using a quartz divider plate in order to prevent parasitic pre-reactions. Before initiating nucleation, the c-plane sapphire substrate was desorbed in situ at high temperature (~1100 °C) for 10 min to prepare the surface. Ga<sub>2</sub>O<sub>3</sub>:Si was then grown for 15 min with a VI/III flow ratio of 324. Silane (SiH<sub>4</sub>) was used as a silicon dopant for *n*-type doping. The thickness of the as-grown Ga<sub>2</sub>O<sub>3</sub>:Si thin film was about 150 nm and the growth rate was  $10 \text{ nm min}^{-1}$ .

After growth, the surface morphology and crystalline structure of the Ga<sub>2</sub>O<sub>3</sub> thin films were studied using scanning electron microscopy (SEM), atomic force microscopy (AFM) and X-ray diffraction (XRD). Figures 1(a) and 1(b) show typical SEM and  $(5 \,\mu\text{m} \times 5 \,\mu\text{m})$  AFM images of postannealed Ga<sub>2</sub>O<sub>3</sub>:Si thin films after annealing in a N<sub>2</sub> atmosphere at 1000 °C for 1 min using a RTA system; for comparison, both insets show the as-grown film surface. The surface morphology of the as-grown Ga<sub>2</sub>O<sub>3</sub>:Si thin films on c-plane sapphire substrates is very uniform and smooth [Figs. 1(a) and 1(b) insets]. Even after high temperature annealing, the surface morphology was maintained, and no cracks were observed that could have been caused by the differing thermal expansion of the  $\beta$ -Ga<sub>2</sub>O<sub>3</sub> film and sapphire substrate. The root-mean-squared (RMS) roughness was measured at 3.4 nm before and 3.0 nm after annealing.

XRD omega/2theta scans of the typical Ga<sub>2</sub>O<sub>3</sub>:Si thin film on c-plane sapphire substrate are shown in Fig. 2(a). Three

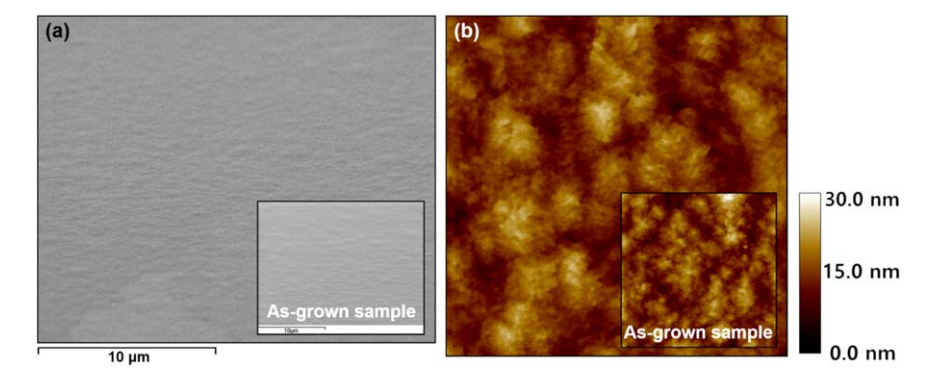


Fig. 1. (Color online) (a) Tilted view SEM image and (b) AFM image (5  $\mu$ m  $\times$  5  $\mu$ m) of post-annealed Ga<sub>2</sub>O<sub>3</sub>:Si thin film. Both insets show the as-grown thin film.

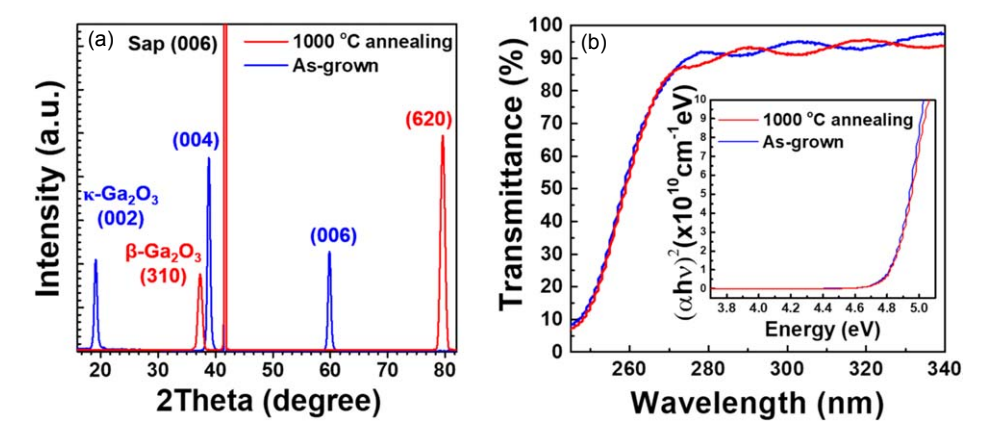


Fig. 2. (Color online) (a) XRD pattern and (b) optical transmission spectra of as grown and after annealing  $Ga_2O_3$ :Si thin film; inset is plot of  $(\alpha h \nu)^2$  versus  $h\nu$ .

sharp peaks (located at  $\sim 18.96^{\circ}$ ,  $\sim 38.84^{\circ}$  and  $\sim 59.76^{\circ}$ ) were observed for the as-grown Ga<sub>2</sub>O<sub>3</sub>:Si thin film. The Ga<sub>2</sub>O<sub>3</sub> associated with these XRD peaks position can typically be either hexagonal  $\varepsilon$ - or orthorhombic  $\kappa$ -phase; exact differentiation between these two phases requires additional nanoscale analysis. We have previously investigated our Ga<sub>2</sub>O<sub>3</sub> as-grown thin films using transmission electron microscopy (TEM) and found them to be κ-Ga<sub>2</sub>O<sub>3</sub>.<sup>21)</sup> These three sharp peaks corresponding to κ-Ga<sub>2</sub>O<sub>3</sub> (002), (004), and (006), respectively, is consistent with a strong preferential (002) orientation along the growth direction. However, after annealing at 1000 °C, XRD clearly shows the phase transforms into monoclinic  $\beta$ -Ga<sub>2</sub>O<sub>3</sub>:Si (310). Fornari et al. reported that similar phase transition occurs in  $\varepsilon$ -phase (002) when  $\varepsilon$ -Ga<sub>2</sub>O<sub>3</sub> thin films is heat treated at a high temperature of 1000 °C with followed by a rapid cooling.<sup>2</sup> Figure 2(b) shows the optical transmission spectra of as grown and post-annealed Ga<sub>2</sub>O<sub>3</sub>:Si thin films and the inset plots  $(\alpha h \nu)^2$  versus  $h \nu$  where  $\alpha$  is the optical absorption coefficient, h is Planck's constant, and  $\nu$  is the photon frequency. As-grown and post-annealed Ga<sub>2</sub>O<sub>3</sub>:Si thin films show a transmission of over 90% for wavelengths above 280 nm. From fitting, the inset of Fig. 2(b) bandgap values were estimated to be 4.82 and 4.83 eV, respectively, for asgrown and post-annealed Ga<sub>2</sub>O<sub>3</sub>:Si thin films. This result indicates that there is no significant change in the bandgap during the phase transition from the  $\kappa$ -phase to the  $\beta$ -phase.

While no significant change occurred in the surface morphology and bandgap of the κ-Ga<sub>2</sub>O<sub>3</sub>:Si thin film after

annealing and phase change to the  $\beta$ -phase, a huge change was observed in the electrical properties as measured by the Hall measurement. The carrier concentration of as-grown sample was  $1.05 \times 10^{16} \, \text{cm}^{-3}$  and the mobility was measured to be as 1.5 cm<sup>2</sup> V<sup>-1</sup>·s<sup>-1</sup> for a dilute (25 ppm) SiH<sub>4</sub> flow of 20 sccm. Unfortunately, for κ-Ga<sub>2</sub>O<sub>3</sub>:Si thin films with SiH<sub>4</sub> flow rates of less than 20 sccm, the electrical characteristics could not be evaluated due to excessively high resistivity. However, after conversion to  $\beta$ -Ga<sub>2</sub>O<sub>3</sub>:Si these low flow-rate films became conductive and Hall characteristics could be evaluated. After phase-transition to  $\beta$ -Ga<sub>2</sub>O<sub>3</sub>:Si decreasing the dilute SiH<sub>4</sub> flow causes the mobility to increase from  $3.1 \text{ cm}^2 \text{ V}^{-1} \cdot \text{s}^{-1}$  to  $22.6 \text{ cm}^2 \text{ V}^{-1} \cdot \text{s}$  and the carrier concentration systematically decrease three orders of magnitude from  $4.2 \times 10^{18} \,\mathrm{cm^{-3}}$  to  $1.3 \times 10^{15} \,\mathrm{cm^{-3}}$  (Fig. 3). The measured mobility values are still relatively low compared to reported cases of Ga<sub>2</sub>O<sub>3</sub> grown on the homo-substrate.<sup>23)</sup> This low value of the mobility is most likely related to the high density of planar defects and in-plane rotational domains when Ga<sub>2</sub>O<sub>3</sub> was grown on the sapphire substrate.<sup>21)</sup> The exact cause of the dramatic change of the electrical characteristics could be the subject of further discussion, but in this letter, we will focus on the characteristics of MOSFET devices fabricated using these thin films.

In order to evaluate the potential of using MOCVD grown  $\beta$ -Ga<sub>2</sub>O<sub>3</sub>:Si on sapphire for power-electronics application, MOSFET devices were fabricated and characterized using the as-grown and post-annealed thin films according to the design shown in Fig. 4. Figures 4(a) and 4(b) show a schematic

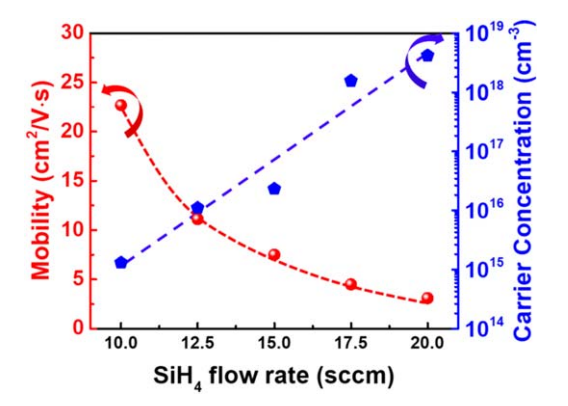


Fig. 3. (Color online) Carrier concentration and mobility of post-annealed  $\beta$ -Ga<sub>2</sub>O<sub>3</sub>:Si thin film as a function of SiH<sub>4</sub> flow rate.

illustration of the cross sectional and isometric view of the  $Ga_2O_3$ :Si MOSFET design. To fabricate the MOSFETs first, a 200  $\mu$ m wide channel was etched by electron cyclotron resonance reactive ion etching (ECR-RIE) for mesa isolation.

Then conventional photolithography and lift-off was used to electron-beam deposit Ti (20 nm)/Au (100 nm) source and drain metal contacts on the MOSFETs. Plasma-enhanced chemical vapor deposition (PECVD) at 350 °C using SiH<sub>4</sub> and NO<sub>2</sub> was used to deposit a 100 nm thick SiO<sub>2</sub> of gate dielectric. The MOSFETs had gate length (L<sub>G</sub>), gate-source spacing (L<sub>GS</sub>), and gate-drain spacing (L<sub>GD</sub>) of 10, 10, and 20  $\mu$ m, respectively, as shown in Fig. 4(c). The gate metal contact [Fig. 4(d)] was then formed by the evaporation of Pt(20 nm)/Ti (20 nm)/Au(100 nm) on the SiO<sub>2</sub> gate. Then, fabricated MOSFETs were tested using a semiconductor parameter analyzer and probe station.

Figure 5(a) shows the DC output I–V ( $I_D$ – $V_{DS}$ ) curves for MOSFET of the  $\kappa$ -Ga<sub>2</sub>O<sub>3</sub>:Si with SiH<sub>4</sub> flow rate 20 sccm from gate voltages ( $V_G$ ) 10 to  $-50\,V$  with a gate step of  $-10\,V$ . A gate voltage ( $V_G$ ) over 10 V was found to degrade the devices. The maximum  $I_D$  is around 9.1 mA mm<sup>-1</sup> at  $V_G = 10\,V$ . Three-terminal breakdown appeared at a  $V_{DS}$  of 390 V with  $V_G = -30\,V$ . The  $I_D$  is effectively modulated by the  $V_G$  as shown in Fig. 5(b). The on/off ratio was measured

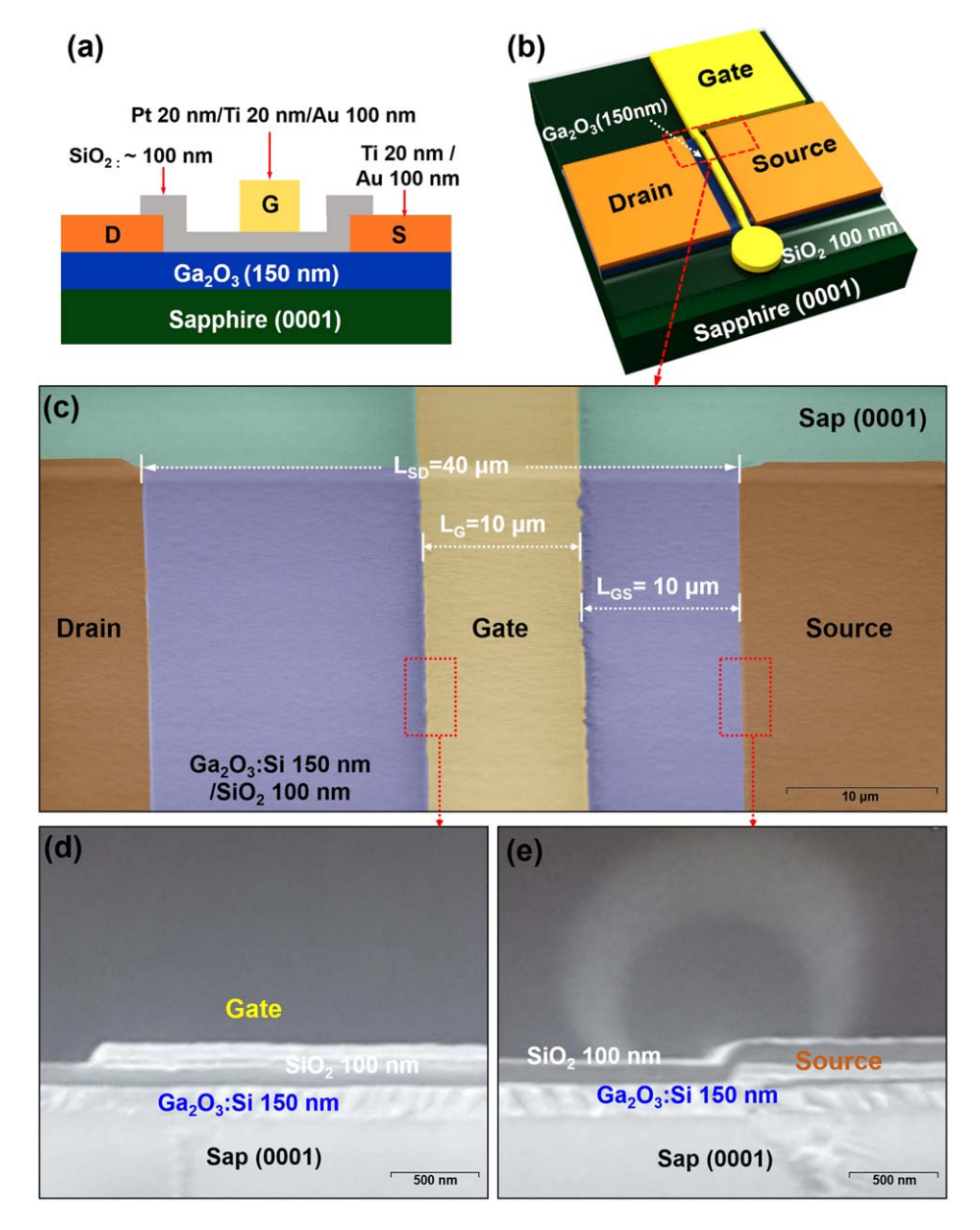


Fig. 4. (Color online) Schematic illustration of the (a) cross sectional and (b) isometric view of Ga<sub>2</sub>O<sub>3</sub>:Si MOSFET design; (c) bird's eye view SEM image of Ga<sub>2</sub>O<sub>3</sub>:Si MOSFET, (d) cross sectional SEM image of gate metal pad and (e) cross sectional SEM image of source metal pad.

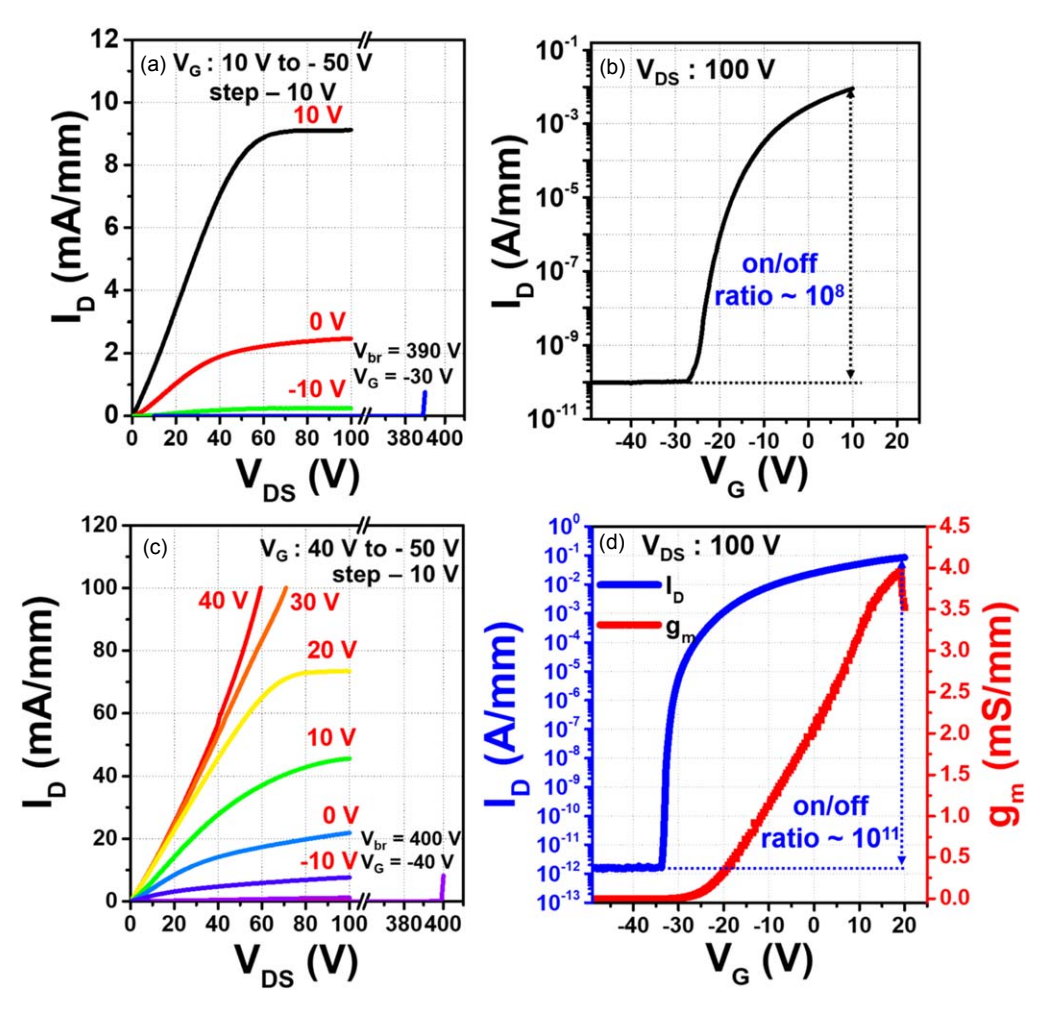


Fig. 5. (Color online) (a) DC I–V characteristics and (b) transfer characteristics of MOSFETs using  $\kappa$ -Ga<sub>2</sub>O<sub>3</sub>:Si with a SiH<sub>4</sub> flow rate 20 sccm; (c) DC I–V characteristics and (d) transfer characteristics of MOSFET using  $\beta$ -Ga<sub>2</sub>O<sub>3</sub>:Si with a SiH<sub>4</sub> flow rate 15 sccm.

as high as  $\sim 10^8$ . MOSFETs fabricated from  $\beta$ -Ga<sub>2</sub>O<sub>3</sub>:Si with various SiH<sub>4</sub> flow rates were then investigated. It was observed that at higher flow rates greater than 17 sccm with high doping concentration, the IV curve is linear. This phenomenon is related to the Mott semiconductor-metal transition and was observed to occur at high doping levels (>  $\sim$ 4 × 10<sup>18</sup> cm<sup>-3</sup>) in Ga<sub>2</sub>O<sub>3</sub>. <sup>24,25)</sup> On the other hand, when the SiH<sub>4</sub> flow rate is less than 5 sccm, drain current only shows a few pA mm<sup>-1</sup> due to the very high channel resistance. The best performance was obtained for β-Ga<sub>2</sub>O<sub>3</sub>:Si MOSFETs fabricated using an intermediate  $SiH_4$  flow of 15 sccm, corresponding to  $\beta$ - $Ga_2O_3$ :Si with an electrical mobility of 7.5 cm<sup>2</sup> V<sup>-1</sup> · s<sup>-1</sup> and a carrier concentration of  $2.3 \times 10^{16} \, \text{cm}^{-3}$ . Figure 5(c) shows the DC output characteristics of this  $\beta$ -Ga<sub>2</sub>O<sub>3</sub>:Si MOSFET at V<sub>G</sub> from 40 to -50 V in steps of -10 V while the  $V_{DS}$  was swept from 0 to 100 V. Degradation did not occur until the gate bias (V<sub>G</sub>) exceeded 40 V. This  $\beta$ -Ga<sub>2</sub>O<sub>3</sub>:Si MOSFET generally shows a 10 times higher maximum I<sub>D</sub> than MOSFETs fabricated from the as-grown  $\kappa$ -Ga<sub>2</sub>O<sub>3</sub>:Si thin film. Because of limitations of our characterization system, the maximum  $I_D$  that we can measure is  $100 \text{ mA mm}^{-1}$  at  $>V_G=30 \text{ V}$ . The three-terminal breakdown voltage in the off state is as high as 400 V at  $V_G = -40 \text{ V}$ . Figure 5(d), demonstrates the depletion mode performance of the device which reveals a high on/off ratio of  $\sim 10^{11}$ . The gate leakage current shows a very low gate leakage current of  $\sim 1.5 \, \mathrm{pA \ mm}^{-1}$ . The on/off ratio value

exhibits a significant improvement of about 3 orders magnitude compared to the as-grown un-annealed thin film. The maximum transconductance ( $g_m$ ) is calculated from transfer characteristic [Fig. 5(d)] to be 3.96 mS mm<sup>-1</sup> and a subthreshold swing (SS) of 210 mV dec<sup>-1</sup> is obtained. The peak field-effect mobility ( $\mu_{FE}$ ) of the device was calculated as well using Eq. (1):

$$\mu_{FE} = \frac{L}{W} \frac{g_m}{V_{DS} C_{OX}} \tag{1}$$

where L and W are the channel length and width, respectively, and  $C_{OX}$  is the oxide capacitance. Using this equation the  $\mu_{\rm FE}$  is calculated to be  $11.4~{\rm cm^2\,V^{-1}\cdot s^{-1}}$ .

In order to give more prospect and comparison of the device performance, Table I summarizes the basic characteristic of  $\beta$ -Ga<sub>2</sub>O<sub>3</sub> FETs on native and sapphire substrate using different methods of growth. According to reported studies up to now,  $\beta$ -Ga<sub>2</sub>O<sub>3</sub> FET devices using native substrate have shown progressive performance improvements by various doping and growth techniques. However, despite the development of  $\beta$ -Ga<sub>2</sub>O<sub>3</sub> thin film growth technology through diverse growth and doping technologies on sapphire substrates, <sup>31,32)</sup> there is not much research performed on  $\beta$ -Ga<sub>2</sub>O<sub>3</sub> MOSFETs on sapphire substrates. Therefore, we believe that this study will lead to a new chapter in research of  $\beta$ -Ga<sub>2</sub>O<sub>3</sub> MOSFETs based on sapphire substrates and other hetero-substrates. The device presented in this work

Substrate On/off ratio  $Max I_D (mA mm^{-1})$  $V_{br}(V)$ References Material growth  $> 10^{10}$ **MBE**  $\beta$ -Ga<sub>2</sub>O<sub>3</sub> 39 370 26 MBE  $10^{4}$ 257 β-Ga<sub>2</sub>O<sub>3</sub> 15 mA 8  $\sim 10^6$ MBE β-Ga<sub>2</sub>O<sub>3</sub> 1.4  $\sim 40$ 27 MBE  $\sim 10^{3}$ 236 15  $\beta$ -Ga<sub>2</sub>O<sub>3</sub> 51  $>1 \text{ kA cm}^{-2}$  $\sim 10^{9}$ **HVPE** 28 β-Ga<sub>2</sub>O<sub>3</sub> 960 MOVPE  $< 10^{2}$ 29 Sapphire 42 nA  $\sim 10^{11}$ MOCVD 400 Sapphire 100 This work  $\sim \! 10^{10}$ SiO<sub>2</sub>/p<sup>++</sup> Si Exfoliation 600 185 18 Exfoliation SiO<sub>2</sub>/p<sup>+</sup> Si  $\sim \! 10^5$ 60  $\sim 100$ 30

**Table I.** Summary of some key parameter in  $\beta$ -Ga<sub>2</sub>O<sub>3</sub> FETs on native and sapphire substrate.

using MOCVD growth, showed the best MOSFET performance among the  $\beta\text{-}Ga_2O_3$  grown on sapphire substrates. These excellent properties are comparable to  $\beta\text{-}Ga_2O_3$  MOSFET devices grown on native substrates and nanomembrane devices. The growth of  $\beta\text{-}Ga_2O_3$ :Si thin films on c-plane sapphire substrates through post-annealing and the improved MOSFET characteristics not only show improved device characteristics, but also demonstrate that  $\beta\text{-}Ga_2O_3$  grown on sapphire has tremendous potential for future power electronic devices.

In summary, we have successfully demonstrated  $\beta$ -Ga<sub>2</sub>O<sub>3</sub>:Si MOSFETs on c-plane sapphire via MOCVD growth. The  $\beta$ -Ga<sub>2</sub>O<sub>3</sub>:Si MOSFETs show a maximum I<sub>D</sub> of 100 mA mm<sup>-1</sup> with an excellent breakdown voltage of 400 V at V<sub>G</sub> = -40 V. The devices exhibit high on/off ratios of  $\sim$ 10<sup>11</sup> with extremely low gate leakage current of  $\sim$ 1.5 pA mm<sup>-1</sup>. Moreover, this excellent performance of  $\beta$ -Ga<sub>2</sub>O<sub>3</sub>:Si MOSFET demonstrated strong potential of the cost effective and scalable MOCVD growth of  $\beta$ -Ga<sub>2</sub>O<sub>3</sub>:Si using low-cost readily available c-plane sapphire substrates for future power electronic device applications.

**Acknowledgments** This material is based upon work supported by the National Science Foundation under Grant No. ECCS-1748339.

ORCID iDs Ji-Hyeon Park 10 https://orcid.org/0000-0002-7114-0065 Arash Dehzangi 10 https://orcid.org/0000-0001-5043-2678 Manijeh Razeghi 10 https://orcid.org/0000-0002-7762-6904

- 1) R. Pohle, E. Weisbrod, and H. Hedler, Procedia Eng. 168, 211 (2016).
- S. Oh, J. Kim, F. Ren, S. J. Pearton, and J. Kim, J. Mater. Chem. C 4, 9245 (2016).
- O. Takayoshi, K. Kaminaga, H. Mashiko, A. Mukai, K. Sasaki, T. Masui, A. Kuramata, S. Yamakoshi, and A. Ohtomo, Jpn. J. Appl. Phys. 52, 111102 (2013)
- L.-X. Qian, H.-F. Zhang, P. T. Lai, Z.-H. Wu, and X.-Z. Liu, Opt. Mater. Express 7, 3643 (2017).
- X. Zhao, W. Cui, Z. Wu, D. Guo, P. Li, Y. An, L. Li, and W. Tang, J. Electron. Mater. 46, 2366 (2017).
- 6) T. Oshima, T. Okuno, N. Arai, N. Suzuki, S. Ohira, and S. Fujita, Appl. Phys. Express 1, 011202 (2008).
- 7) D. Guo et al., Opt. Mater. Express 4, 1067 (2014).

- M. Higashiwaki, K. Sasaki, A. Kuramata, T. Masui, and S. Yamakoshi, Appl. Phys. Lett. 100, 013504 (2012).
- M. Higashiwaki, K. Sasaki, A. Kuramata, T. Masui, and S. Yamakoshi, Phys. Status Solidi A 211, 21 (2014).
- 10) Z. Galazka et al., J. Cryst. Growth 404, 184 (2014).
- 11) Q. Feng, X. Li, G. Han, L. Huang, F. Li, W. Tang, J. Zhang, and Y. Hao, Opt. Mater. Express 7, 1240 (2017).
- H. von Wenckstern, D. Splith, M. Purfürst, Z. Zhang, C. Kranert, S. Müller,
  M. Lorenz, and M. Grundmann, Semicond. Sci. Technol. 30, 024005 (2015).
- 13) K. Sasaki, M. Higashiwaki, A. Kuramata, T. Masui, and S. Yamakoshi, Appl. Phys. Express 6, 086502 (2013).
- 14) M. Higashiwaki, H. Murakami, Y. Kumagai, and A. Kuramata, Jpn. J. Appl. Phys. 55, 1202A1-1-7 (2016).
- 15) S. Krishnamoorthy, Z. Xia, S. Bajaj, M. Brenner, and S. Rajan, Appl. Phys. Express 10, 051102 (2017).
- 16) K. Zeng, A. Vaidya, and U. Singisetti, IEEE Electron Device Lett. 39, 1385 (2018).
- 17) Y. Lv et al., IEEE Electron Device Lett. 40, 83 (2018).
- 18) H. Zhou, M. Si, S. Alghamdi, G. Qiu, L. Yang, and P. D. Ye, IEEE Electron Device Lett. 38, 103 (2017).
- 19) J. Kim, S. Oh, M. A. Mastro, and J. Kim, Phys. Chem. Chem. Phys. 18, 15760 (2016).
- 20) Z. Li, Y. Liu, A. Zhang, Q. Liu, C. Shen, F. Wu, C. Xu, M. Chen, H. Fu, and C. Zhou, Nano Res. 12, 143 (2019).
- 21) Y. Xu, J. Park, Z. Yao, C. Wolverton, M. Razeghi, J. Wu, and V. P. Dravid, ACS Appl. Mater. Interfaces 11, 5536 (2019).
- 22) R. Fornari et al., Acta Mater. 140, 411 (2017).
- 23) Z. Feng, A. F. M. Anhar Uddin Bhuiyan, M. R. Karim, and H. Zhao, Appl. Phys. Lett. 114, 250601 (2019).
- 24) S. Rafique, L. Han, S. Mou, and H. Zhao, Opt. Mater. Express 7, 3561 (2017).
- E. Chikoidze, H. J. Von Bardeleben, K. Akaiwa, E. Shigematsu, K. Kaneko,
  S. Fujita, and Y. Dumont, J. Appl. Phys. 120, 025109 (2016).
- 26) M. Higashiwaki, K. Sasaki, T. Kamimura, M. Hoi Wong, D. Krishnamurthy, A. Kuramata, T. Masui, and S. Yamakoshi, Appl. Phys. Lett. 103, 123511 (2013).
- 27) M. H. Wong, Y. Nakata, A. Kuramata, S. Yamakoshi, and M. Higashiwaki, Appl. Phys. Express 10, 041101 (2017).
- 28) Z. Hu et al., Appl. Phys. Lett. 113, 122103 (2018).
- 29) M. J. Tadjer et al., J. Electron. Mater. 45, 2031 (2016).
- 30) S. Ahn, F. Ren, J. Kim, S. Oh, J. Kim, M. A. Mastro, and S. J. Pearton, Appl. Phys. Lett. 109, 062102 (2016).
- 31) S. Rafique, M. R. Karim, J. M. Johnson, J. Hwang, and H. Zhao, Appl. Phys. Lett. 112, 052104 (2018).
- 32) M. Baldini, M. Albrecht, A. Fiedler, K. Irmscher, R. Schewski, and G. Wagner, ECS J. Solid State Sci. Technol. 6, O3040 (2017).
- 33) H. Dong, H. Xue, Q. He, Y. Qin, G. Jian, S. Long, and M. Liu, J. Semicond. 40, 011802 (2019).